Smart Structures and Systems, Vol. 4, No. 5 (2008) 531-548
DOI: http://dx.doi.org/10.12989/sss.2008.4.5.531

Inductively coupled nanocomposite wireless strain and pH sensors

Kenneth J. Loh*, Jerome P. Lynch‡ and Nicholas A. Kotov‡†

The University of Michigan, Ann Arbor, MI 48109-2125, USA

(Received March 23, 2007, Accepted November 5, 2007)

Abstract. Recently, dense sensor instrumentation for structural health monitoring has motivated the need for novel passive wireless sensors that do not require a portable power source, such as batteries. Using a layer-by-layer self-assembly process, nano-structured multifunctional carbon nanotube-based thin film sensors of controlled morphology are fabricated. Through judicious selection of polyelectrolytic constituents, specific sensing transduction mechanisms can be encoded within these homogenous thin films. In this study, the thin films are specifically designed to change electrical properties to strain and pH stimulus. Validation of wireless communications is performed using traditional magnetic coil antennas of various turns for passive RFID (radio frequency identification) applications. Preliminary experimental results shown in this study have identified characteristic frequency and bandwidth changes in tandem with varying strain and pH, respectively. Finally, ongoing research is presented on the use of gold nanocolloids and carbon nanotubes during layer-by-layer assembly to fabricate highly conductive coil antennas for wireless communications.

Keywords: carbon nanotubes; layer-by-layer; nanocomposite; pH sensing; RFID; strain sensor; structural monitoring.

1. Introduction

Around the world, civil infrastructures such as buildings, bridges, lifelines, among others, represent the foundation for economic welfare and societal prosperity. Many of these vital structures are beginning to approach (or have already exceeded) their design service lifetimes. Today, $91 billion is spent annually to maintain the U.S. inventory of highways and bridges; however, an additional $128 billion is needed to upgrade existing structures to current standards (Njord and Meyer 2006). As such, efficient and cost-effective strategies are required to ensure infrastructure serviceability and safety. In most cases, the current state of practice relies on schedule-based maintenance routines in which engineers rely on visual inspection to assess structural performance. Not only is this method subjective (Moore, *et al*. 2001), but a schedule-based maintenance program is often economically inefficient, as newer structures may not need inspection during their initial years of service.

As a result, many researchers have proposed tethered sensor networks for monitoring structural performance over time, commonly termed structural health monitoring (SHM). Using a few distributed

*Department of Civil and Environmental Engineering
‡Assistant Professor, Department of Civil and Environmental Engineering & Department of Electrical Engi neering and Computer Science
‡†Department of Chemical Engineering

sensors (e.g. accelerometers) installed within the civil infrastructure then coupled with automated damage detection algorithms at the centralized data repository, a comprehensive SHM system can be formed (Doebling, *et al*. 1998). Structural health monitoring can objectively monitor long-term structural reliability and serviceability. However, the high costs to install and maintain the extensive coaxial cables connecting sensors to the centralized data repository have warranted novel cost-effective methods for SHM. For example, the cost to install tethered sensors in tall buildings and long bridges can exceed thousands of dollars on a per channel basis (Celebi 2002, Farrar 2001). High system costs result in low sensor densities in large-scale civil infrastructures; as a result, generally only global vibration characteristics are deduced from so few sensors. Nevertheless, the advent of tethered sensors for SHM has initiated the shift from schedule-based to performance-based monitoring.

Instead of using cable-based sensors for global vibration structural characterization, a variety of academic and commercial wireless sensor networks have been proposed for densely distributed SHM systems (Straser and Kiremidjian 1998, Spencer, *et al*. 2004, Lynch and Loh 2006). Costing approximately $100 per sensing node, low wireless sensor costs permit high nodal densities for component-level damage detection (e.g. monitoring strain and corrosion processes). Furthermore, with local computational power embedded within each sensor node, distributed data processing (Lynch, *et al*. 2003, Tanner, *et al*. 2003) and wireless structural control (Loh, *et al*. 2007a) have been achieved. Numerous field validation studies conducted with wireless sensors have indicated performance levels comparable with traditional cable-based monitoring systems (Lynch, *et al*. 2006). Unfortunately, one significant disadvantage of the aforementioned wireless sensors is their inherent dependency on power supplies (e.g. batteries or AC power source). To conserve power, some researchers have adopted trigger-based power-on mechanisms (i.e. when acceleration exceeds a preset threshold) (Straser and Kiremidjian, 1998) as well as local data processing to solely transfer computed results (as opposed to the entire time history record) to reduce power consumed by the wireless transceiver (Lynch and Loh 2006). These efforts have only led to moderate improvements in sensor service lifetimes with life expectancy to approximately two years. Furthermore, while methods for converting ambient mechanical vibration into electrical energy are currently underway (Sodano, *et al*. 2004), the field of power harvesting is still in its infancy.

In order to preserve the advantages offered by wireless sensing while simultaneously addressing issues regarding power limitations, some researchers have adopted inductively coupled radio frequency identification (RFID) sensing systems for strain and corrosion monitoring. Through the use of a coil antenna wirelessly coupled to an AC (alternating current) generator (i.e. the reader), the reader can inductively power and communicate with a remote passive sensor circuit in close proximity (Finkenzeller 2003). Early investigatory work in RFID sensing has been proposed by Mita and Takahira (2002, 2003) where they have developed a passive wireless peak strain sensor based on two concentric aluminum pipes sliding over a dielectric material. Upon installing these sensors to the base of a seven-story base-isolated building at Keio University, experimental peak strain data collected from the prototype RFID sensor coincides with those obtained from a laser displacement transducer (Mita and Takahira 2004). Extension to Mita and Takahira's work proposed by Todd (2005) seeks the utilization of MEMS (microelectromechanical systems) processes to miniaturize the capacitive peak strain sensor. As opposed to measuring peak strain, Jia and Sun (2006) have developed a novel passive thick film strain sensor by incorporating poly(vinyl fluoride) with an interdigital capacitor to enhance the sensitivity of characteristic frequency shifts to strain. On the other hand, for monitoring corrosion processes, Bernhard, *et al*. (2003) have developed a 2.4 GHz RFID wireless sensor to detect the loss of interfacial bond strength and reduction in steel-reinforcement cross-sectional area in concrete via

acoustic emissions. To accurately monitor different thresholds of concrete corrosion wirelessly, Simonen, *et al*. (2004) utilize an exposed switch fabricated with different gauge steel wires. When corrosion destroys the exposed wire switch, dramatic characteristic frequency shifts have been observed between initial and corroded states. Unfortunately, among the wide variety of RFID-based strain and corrosion sensors that exist, most have a large form factor and are derived by miniaturizing mechanical elements.

In this study, a prototype thin film passive wireless strain and pH sensor is proposed for localized strain and corrosion monitoring. Encoding of electromechanical and electrochemical sensing transduction mechanisms (i.e. strain and pH, respectively) within a thin film structure is accomplished by adopting material fabrication techniques derived from the nanotechnology domain. Nanotechnology provides novel tools and materials such that, by manipulating material properties at the molecular scale, one can utilize a "bottom-up" design methodology to yield high performance sensors. In particular, single-walled carbon nanotubes (SWNTs) and a variety of polyelectrolyte (PE) species combined with a layer-by-layer (LbL) fabrication technique can produce a homogeneous multilayer thin film sensor of controlled morphology. When coupled with a coil antenna, the final multifunctional sensor package is capable of wirelessly detecting strain and pH via characteristic frequency and bandwidth changes, respectively. Preliminary experimental laboratory validation studies are presented to characterize the performance attributes of this wireless multifunctional SWNT-PE composite sensor.

2. RFID sensing systems

Among the wide variety of radio frequency identification systems available, the simplest is the passive RFID system which consists of a reader and a remote tag or transponder. The RFID reader is powered by an AC source and is responsible for wirelessly transmitting power and receiving sensor data from the tag, all through inductive coupling. While many commercial and academic RFID tags are coupled with digital electronics (e.g. electronic microchips) for use in a variety of smart card applications, digital electronics will not be used in this study. Any change in sensor response will cause the fundamental properties of the RFID system to change, namely the characteristic frequency and bandwidth of the reader-tag coupling.

2.1. The reader

In its simplest form, a typical RFID reader consists of a coil antenna connected to an automatic frequency response analyzer (FRA). In this study, the Solartron 1260 impedance gain/phase analyzer is selected for its ease of use and its ability to measure electrical impedance in a frequency range between 100 mHz to 32 MHz (well within the operating frequency range of the proposed RFID sensor system, as will be discussed later). When measuring the complex-valued impedance, Z ($Z = A + jB$ where A and B are the real and imaginary components of the impedance, respectively), the FRA generates a regulated AC voltage signal that is applied to the reader coil; simultaneously, the FRA measures the corresponding AC current response in the coil as AC frequency, f, is varied. As the AC sinusoidal signal passes through the reader coil antenna, a magnetic field is generated in the vicinity of the reader's coil as can be calculated by Eq. (1) and depicted in Fig. 1 (for a circular reader coil based on Faraday's Law) (Finkenzeller 2003).

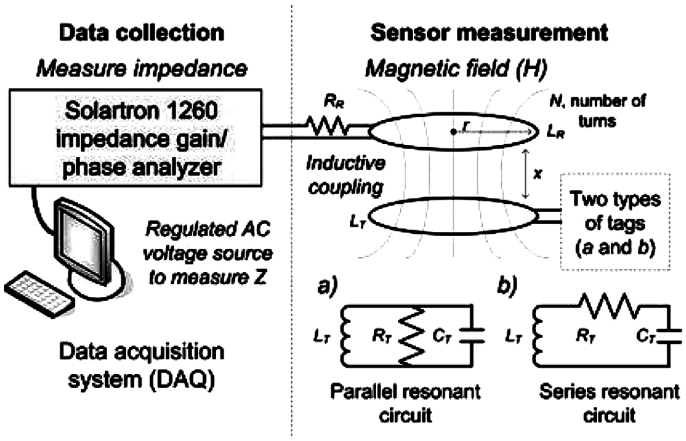

Fig. 1 A schematic illustrating RFID wireless interrogation of a (a) parallel or (b) series resonant tag

$$H = \frac{I \cdot N \cdot r^2}{2\sqrt{(r^2 + x^2)^3}} \tag{1}$$

where I is the current passing through the coil, r is the antenna radius, N is the number of turns, and x is the read-distance along the central axis of the coil (Fig. 1). This resulting magnetic field is employed to induce current and a potential drop in an RFID tag within close proximity. From Eq. (1), it can be observed that a tradeoff exists between different size antennas such that smaller antennas are capable of generating higher fields at the coil axis but larger antennas generate higher magnetic fields over larger distances (x).

2.2. Sensor tag

Typically, the circuitry of a basic sensor tag consists of a resistor (R_T), inductor (coil antenna) (L_T), and capacitor (C_T) in a parallel or series resonant circuit configuration, also known as an RLC-circuit (Figs. 1 and 2). Inherent to each parallel or series resonant circuit are two quantities, namely its characteristic (or resonant) frequency (f_n) and bandwidth (B). While the characteristic frequency of an RLC-circuit does not change with circuit configuration, bandwidth varies between a parallel and series resonant circuit as shown in Eqs. (2) and (3).

$$f_n = \frac{1}{2\pi\sqrt{L_T C_T}} \tag{2}$$

$$B_{series} = \frac{R_T}{2\pi L_T} \tag{3a}$$

$$B_{parallel} = \frac{1}{2\pi R_T C_T} \tag{3b}$$

Selection of sensor tag circuit configuration depends on whether characteristic frequency shift or bandwidth change is more desirable. Furthermore, certain voltage and current requirements for powering onboard

digital electronics governs the type of resonant circuit configuration used. At resonance (f_n), series and parallel tags provide maximum current (minimum impedance) or maximum voltage (maximum impedance), respectively (Lee 1998).

2.3. Coupled reader and tag system

If the Solartron 1260 FRA measures the complex impedance response of the reader coil antenna, the measured impedance would be governed by Eq. (4).

$$Z = R_R + j\omega L_R \tag{4}$$

where R_R is the inherent series resistance of the coil, L_R is the inductance of the reader coil antenna, and ω (rad/sec) is the natural cyclic frequency of the input AC sinusoidal signal (Fig. 2a). However, when a sensor tag comes in the vicinity of the reader coil, an additional complex impedance term (due to inductive coupling, Z_T') is superimposed onto the impedance of the measured coil antenna.

$$Z = R_R + j\omega L_R + Z_T' \tag{5}$$

In order to calculate Z_T', one can begin by calculating the equivalent impedance of each circuit element in the series or parallel sensor tag: namely, the inductor (Z_L), resistor (Z_R), and capacitor (Z_C) impedances:

$$\begin{aligned} Z_L &= R_S + j\omega L_T \\ Z_R &= R_T \\ Z_C &= \frac{1}{j\omega C_T} \end{aligned} \tag{6}$$

Note, the resistance R_S is the inherent series resistance of the sensor tag's inductive coil. Using the equivalent impedance of each circuit element as given in Eq. (6), the total impedance measured at the reader can be determined. For example, when a series resonant circuit tag comes into close proximity to the RFID reader, the measured impedance can be calculated by Eq. (7).

$$Z = R_R + j\omega L_R + \frac{k^2\omega^2 L_R L_T}{Z_L + Z_C + Z_R} \tag{7}$$

Similarly, for a parallel resonant circuit:

$$Z = R_R + j\omega L_R + \frac{k^2\omega^2 L_R L_T}{1/Z_L + 1/Z_C + 1/Z_R} \tag{8}$$

From Eqs. (7) and (8), a coupling factor (k, a number between 0 and 1) qualitatively describes the mutual inductance between the reader and sensor coil antennas. Theoretically, $k = 1$ when the reader and tag coil antennas are of the same size, the same inductance, perfectly aligned by their coil axes, and separated by a distance of zero. However, the coupling factor is strongly dependent on coil geometry, operating conditions, range, among other factors. In the event that no sensor tag is present (where the

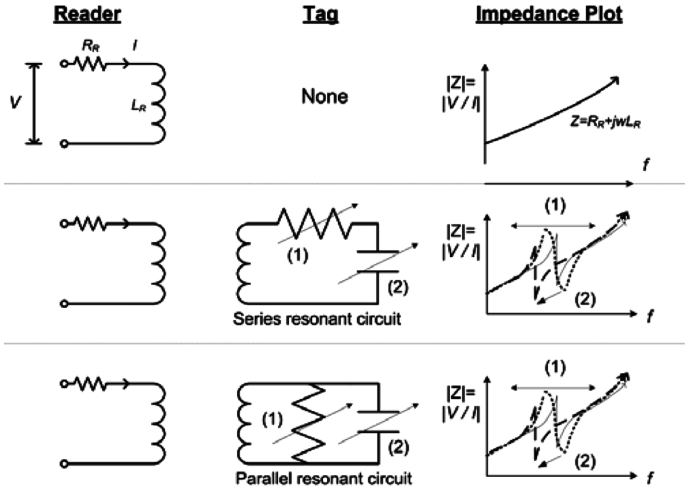

Fig. 2 A schematic illustrating RFID reader impedance (Z) response when no sensor tag is in the vicinity or when present with a series or parallel resonant circuit. A resistance or capacitance change will cause bandwidth (1) and resonant frequency (2) to change, respectively

distance between the coils can be approximated by infinity), $k = 0$, and Eqs. (7) and (8) reduce back to Eq. (4).

In this study, incorporation of sensors with RFID tag technology is accomplished by using parallel resonant circuit configurations. Using resistive or capacitive sensors, the reader can detect changes in bandwidth or characteristic frequency as shown in Fig. 2. For instance, if a capacitive strain sensor is employed, any increase in capacitance will result in a decrease in resonant frequency that can be modeled using Eq. (2). Similarly, an RFID sensor can be designed based on changes in the tag resistor resulting in changes to the reader-tag bandwidth.

3. Layer-by-layer sensor fabrication

Fabrication of multifunctional carbon nanotube-polyelectrolyte composite thin films is accomplished using a layer-by-layer (LbL) self-assembly methodology (Decher 1997, Kotov 2001). Through the sequential dipping of a charged substrate (e.g. glass, silicon, poly(ethylene terephthalate)) in oppositely charged polycationic and polyanionic solutions, different species such as carbon nanotubes, polyelectrolytes, and nanoparticles can be deposited one monolayer at a time (Fig. 3). To begin LbL thin film fabrication, a clean glass microscope slide treated with piranha solution (3:7 by vol. H_2O_2:H_2SO_4) is dipped into a polycationic solution (1.0 wt.% poly(vinyl alcohol) (PVA, Sigma) or 1.0 wt.% poly(aniline) emeraldine base (PANI, Aldrich)) for 5 min to deposit the initial monolayer. Upon rinsing with 18 MΩ deionized water (Millipore) (3 min) followed by drying with compressed nitrogen (10 min), the slide is then immersed in a polyanionic solution (SWNTs dispersed in 1.0 wt.% poly(sodium 4-styrene sulfonate) (PSS, 1,000,000 M_w, Aldrich)) to deposit the next monolayer. Similarly, after a dipping time of 5 min, the glass slide and the adsorbed monolayer is rinsed in 18 MΩ deionized water for 3 min and dried for 10 min. This process completes the fabrication of one bilayer of the thin film; through repetition of the aforementioned process, the end result is a homogeneous multilayer thin film of controlled morphology denoted as $(A/B)_n$ (where A and B represent the oppositely charged species, and n denotes the number of

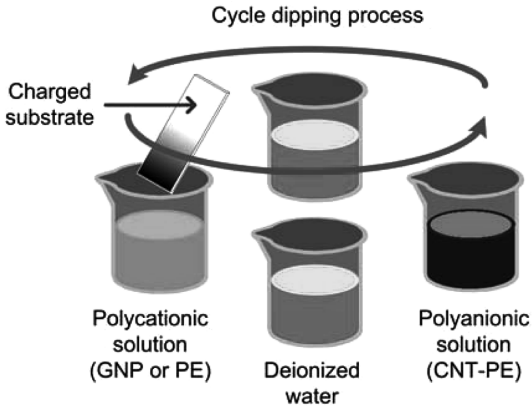

Fig. 3 A schematic illustrating the layer-by-layer self-assembly process

film bilayers).

As outlined in Loh, *et al*. (2007b), different sensing transduction mechanisms (e.g. strain, pH, temperature, light, among others) can be encoded within LbL thin films through the judicious selection of polyelectrolyte species. In this study, single-walled carbon nanotubes (0.8 mg/mL) dispersed in 1.0 wt.% PSS is employed as the polyanionic solution for LbL thin film fabrication. Similar to Loh, *et al.* (2007b), steric stabilization of nanotubes in PSS can be achieved by subjecting the SWNT-PSS solution to 90 min of an ultrasonic bath (135 W, 42 kHz) followed by 90 min of high-powered probe sonication (3.178 mm tip, 30% amplitude, 750 W, 22.0 kHz). For the polycationic solution, two different polyelectrolytes, namely PVA deposited on PET substrates and PANI deposited on glass substrates, are employed to yield capacitive strain sensors and resistive pH sensors, respectively. Table 1 outlines the LbL constituents required for fabricating SWNT-PE strain and pH sensors.

4. Experimental results and discussion

Provided the extreme versatility of LbL-fabricated carbon nanotube composite thin films, the films are employed as integral elements of passive wireless sensors based on RFID technology. Two sensors are specifically proposed: strain and pH sensors. A carbon nanotube composite film is deposited on a soft substrate to act as the variable capacitor (sensitive to strain) of a parallel RFID sensor tag. Second, a PANI-based thin film is employed as a variable resistor (sensitive to pH) in an RFID tag. Both sensors proposed employ traditional inductive coils constructed from 28 AWG magnetic coil wire. Preliminary

Table 1 Summary of layer-by-layer thin film sensor constituents

Sensor Type	Mechanism	Substrate	Polycationic specie	Polyanionic specie
Strain sensing	Capacitive	Poly(ethylene terephthalate)	1.0 wt.% Poly(vinyl alcohol)	1.0 mg/mL SWNT in 1.0 wt.% Poly(sodium 4-styrene sulfonate)
pH sensing	Resistive	Glass (SiO_2)	1.0 mg/mL Poly(aniline) (emeraldine base) in 10 vol. % N,N-dimethyl formamide	1.0 mg/mL SWNT in 1.0 wt.% Poly(sodium 4-styrene sulfonate)

work in depositing inductive coil antennas directly in the LbL process is presented.

4.1. Wireless strain sensing

In a recent study conducted by Loh, *et al*. (2007b), $(SWNT\text{-}PSS/PVA)_n$ thin films have been demonstrated to exhibit piezoresistive response under applied tensile-compressive strains ($\varepsilon = \pm 10{,}000$ μm/m). Despite their ability to precisely tailor strain sensor sensitivity by adjusting initial fabrication parameters, the strain sensor response exhibits a time-dependent exponential decay in film resistance. It is hypothesized that applied electrical current (used for measuring resistance) induces permanent chemical and physical changes at nanotube-to-nanotube junctions, thereby increasing film conductivity over time (Loh, *et al*. 2008). To avoid gradual conductive changes to interfere with the sensor reading, an alternative approach is taken. The conductive carbon nanotube thin film is deposited by LbL on a soft polymeric substrate. The thin film and substrate, under applied strain, will exhibit a change in capacitance directly correlated to strain.

The design of an LbL SWNT-based capacitive strain sensor is accomplished using a charged PET substrate (0.127 mm thick). By depositing $(SWNT\text{-}PSS/PVA)_{100}$ thin films on both sides of this flexible PET thin film, an SWNT-based parallel-plate capacitive strain sensor can be formed as depicted in Fig. 4 (denoted as SWNT-on-PET). PET is selected as the dielectric layer due to its high Poisson's ratio (*ca* 0.4) and ductility. Thus, the capacitance of the SWNT-on-PET strain sensor under applied strain can be calculated via Eq. (9).

$$C_{SWNT-on-PET} = \frac{\varepsilon_r \varepsilon_0 w L}{g}(1 + \varepsilon_s) \tag{9}$$

where ε_r is the relative dielectric permittivity of PET, ε_0 is the permittivity of air ($\varepsilon_0 = 8.854 \cdot 10^{-12}$ F/m), w (width) and L (length) are the dimensions of the parallel-plate capacitor, g is the initial thickness of the PET thin film substrate (0.127 mm), and ε_s is the applied strain. From Eq. (9), it is obvious that capacitance is linearly proportional to applied strain. Furthermore, sensor capacitance can be precisely tuned by controlling sensor dimensions (w, L, and g). Upon coupling this capacitive strain sensor with a parallel resonant tag circuit (where $L \approx 235$ μH and $R \approx 1.2$ MΩ), any applied strain will result to an inversely proportional shift in resonant frequency as given in Eq. (2). The inductive tag element is assembled by a wire coil approximately 45 mm in radius and 50 turns.

Validation of this wireless strain sensor is conducted by applying one cycle of a tensile-compressive

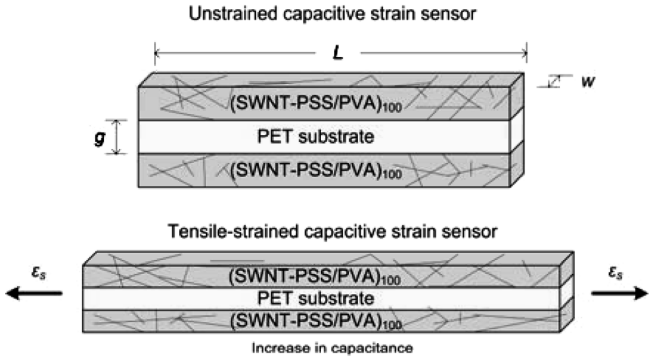

Fig. 4 Conceptual illustration showing how strain affects thin film dimensions that lead to capacitance change

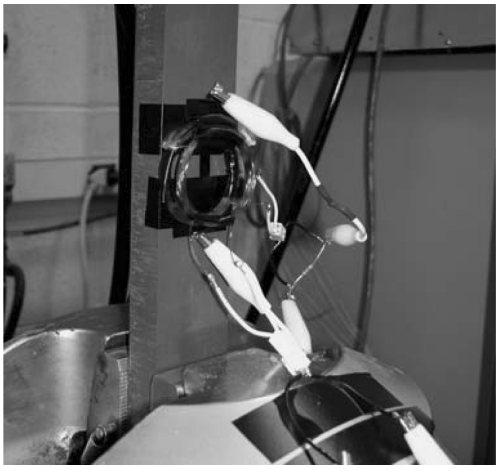

Fig. 5 SWNT-on-PET capacitive strain sensor (epoxy-bonded to a PVC bar) in a parallel resonant circuit configuration loaded by the MTS-810 load frame

load pattern ($\varepsilon = \pm 10{,}000$ μm/m) while wirelessly measuring its response using the Solartron 1260 impedance gain/phase analyzer coupled with a coil antenna to form the RFID reader. Prior to mechanical loading, the wireless strain sensor is mounted to a poly(vinyl chloride) (PVC Type I) rectangular tensile coupon (31 cm long, 4 cm wide, 2 cm thick) via standard CN-E strain gauge epoxy (Tokyo Sokki Kenkyujo) as shown in Fig. 5. Upon sufficient drying (6 hours), an MTS-810 load frame is employed to apply the one-cycle tensile-compressive load pattern at 2,500 μm/m strain increments. At each strain increment, the load frame is held at constant displacement and load (for approximately 5 min) to allow the RFID reader to wirelessly interrogate the strain sensor tag. The distance between the reader and tag coils is approximately 3 cm.

Fig. 6 represents a typical experimental data plot of the wireless strain sensor's coupled impedance as

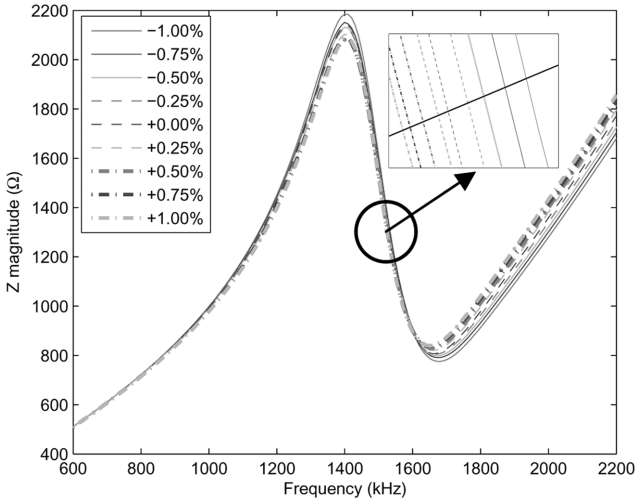

Fig. 6 Experimental RFID reader response of SWNT-on-PET capacitive strain sensor under one-cycle tensile-compressive cyclic loading to ±10,000 μm/m (inset shows zoomed in plot near the resonant frequency)

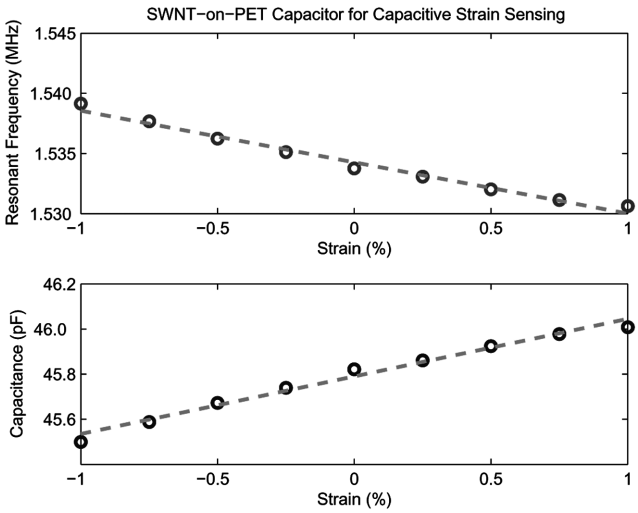

Fig. 7 (a) Resonant frequency shift of SWNT-on-PET capacitive strain sensor under one-cycle tensile-compressive cyclic loading to ±10,000 μm/m; (b) corresponding SWNT-on-PET capacitance change

collected by the RFID reader. Identification of sensor characteristic frequency can be accomplished by observing a dip in the phase angle or the inflection point in the impedance magnitude-frequency plot (Simonen, *et al*. 2004). Fig. 7(a) plots the experimentally determined resonant frequency as a function of applied strain. From substituting Eq. (9) into Eq. (2) to yield Eq. (10), it is apparent that resonant frequency shift is nonlinearly related to applied strain (i.e. by a $1/\sqrt{(1+\varepsilon_s)}$ relationship).

$$f_n = \frac{1}{2\pi\sqrt{L_T\varepsilon_r\varepsilon_0 wL(1+\varepsilon_s)/g}} \tag{10}$$

Nevertheless, since the degree of nonlinearity is small, strain sensor sensitivity (S_C) can be approximated by fitting a linear least-squares best-fit line to Fig. 7(a) to yield $S_C = 0.427$ Hz/μm-m^{-1}. It should be noted that because the differential frequency step during impedance measurement is small ($\Delta f = 1$ kHz), linear interpolation is employed between data points to extract sensor resonant frequency at each applied strain increment. Furthermore, upon determining sensor characteristic frequency, capacitance is back-calculated using Eq. (2) and plotted in Fig. 7(b). Apparent in Fig. 7(b), capacitance does indeed increase linearly in tandem with applied strain (as expected based on Eq. (9)).

4.2. Wireless pH sensing

As opposed to using a capacitive-based sensor for monitoring strain, a resistive thin film pH sensor is employed for wireless pH sensing. Similar to Loh, *et al*. (2007b) and as outlined in Section 3 of this paper, LbL (SWNT-PSS/PANI)$_n$ thin films exhibit pH sensitivity. To characterize (SWNT-PSS/PANI)$_n$ thin film pH sensing performance, an initial study to measure change in film resistance under a wide range of pH buffer solutions (pH 1-10) is conducted. Using (SWNT-PSS/PANI)$_{50}$ thin films still attached to their original glass substrate, these films are cut with a diamond-tipped scriber into small rectangular specimens (7 mm by 11 mm). A plastic well is attached to the center of the film surface via

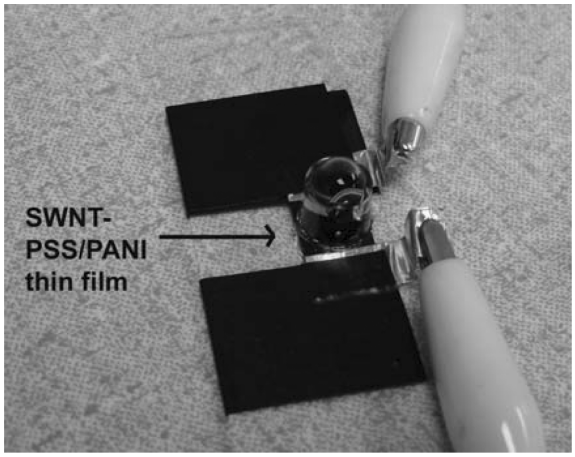

Fig. 8 $(SWNT\text{-}PSS/PANI)_{50}$ thin film with plastic well mounted for pipetting pH buffer solutions

high-vacuum grease (Dow Corning), thereby allowing different pH buffer solutions to be pipetted into this plastic well. Finally, electrical connections are established by drying colloidal silver paste (Ted Pella) over single-strand wire at the two ends of the thin film as shown in Fig. 8.

Characterization of $(SWNT\text{-}PSS/PANI)_{50}$ thin film pH sensor performance begins by pipetting increasing pH buffer solutions while measuring film resistance with an Agilent 34401A digital multimeter connected in a two-point probe fashion. While a two-point probe method is subjective to contact resistance issues, contact resistance is negligible since typical film resistance is on the order of 10^1 to 10^3 kΩ. Fig. 9(a) plots the $(SWNT\text{-}PSS/PANI)_{50}$ thin film resistance time history when subjected to incremental pH buffer solutions (where $\Delta pH = 1$). It can be observed that the pH sensor exhibits dramatic increases in resistance in tandem with increasing pH. By plotting the change in film resistance as a function of pH buffer solution, it can be concluded that the pH response is near-linear (Fig. 9b). In

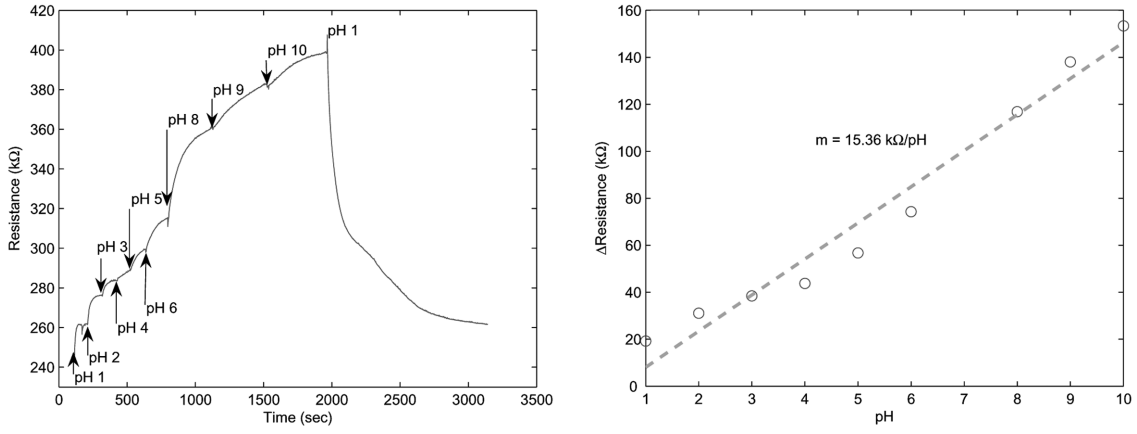

(a) (b)

Fig. 9 (a) Time history plot of $(SWNT\text{-}PSS/PANI)_{50}$ thin film resistance due to different pH buffer solutions. (b) Linearity plot depicting the change of resistance as a function of applied pH buffer solution indicating pH sensing sensitivity is 15.36 kΩ/pH

addition, by fitting a linear least-squares best-fit line, pH sensitivity (S_{pH}) can be calculated using Eq. (11) (equivalent to the slope of the best-fit line).

$$S_{pH} = \frac{\Delta R / A}{\Delta pH} \tag{11}$$

where A is the area of the thin film for normalization purposes. For this particular thin film, pH sensitivity is approximately 19.9 kΩ-cm^{-2}/pH (in agreement with those obtained by Loh, *et al*. 2007b). Furthermore, from Fig. 9(a), it is apparent that the (SWNT-PSS/PANI)$_{50}$ pH sensor is fully reversible; upon pipetting a pH 10 solution, the addition of a pH 1 solution will renormalize thin film nominal resistance.

Since nominal film resistance is high (10^1 to 10^3 kΩ), (SWNT-PSS/PANI)$_{50}$ thin films are coupled with a parallel resonant circuit consisting of a 2,100 μH inductive coil antenna and a 220 pF tuning capacitor to achieve wireless pH sensing. Here, the inductive coil is a 80 mm radius coil consisting of 90 turns. This circuit configuration will cause a change in system bandwidth due to different pH buffer solutions inducing a change in film resistance (from Eq. (3b)). Similar to the aforementioned wireless strain sensor, the resulting pH sensor response is nonlinear, exhibiting a $1/R_T$ relationship between bandwidth and film resistance.

For wireless sensor interrogation, the Solartron 1260 impedance gain/phase analyzer connected to an inductive coil antenna is employed as the RFID reader. Again, pH buffer solutions (pH 1-10) are individually pipetted into the plastic well (Fig. 8). Upon the addition of a pH buffer solution, the RFID reader is employed to measure the complex impedance over a range of frequencies. Once the RFID reader completes interrogating the pH sensor tag, the pH buffer solution in the plastic well is removed, and immediately, a different pH buffer solution is pipetted in. A representative experimental overlay is shown in Fig. 10.

The inset of Fig. 10, which shows a zoomed-in portion of the experimental impedance magnitude-frequency overlay, indicates that system bandwidth decreases with increasing pH buffer solutions.

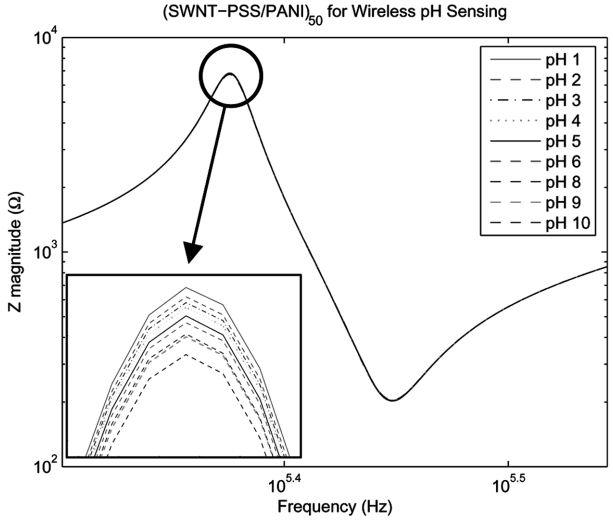

Fig. 10 Impedance magnitude-frequency response as measured by the Solartron 1260 reader to capture the wireless pH sensor performance with different pH buffer solutions

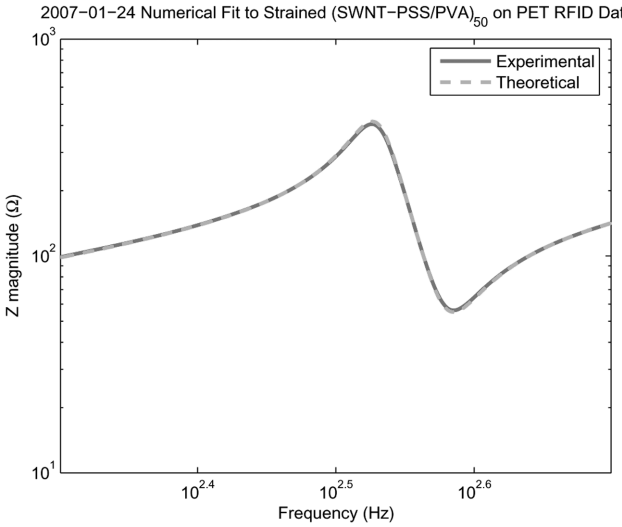

Fig. 11 Validation of stochastic simulated annealing model-fitting between theoretical and experimental RFID reader response indicates good fit

However, bandwidth is inherently difficult to quantify; although one can subjectively select frequency limits and calculate bandwidth, this method does not correlate with theory as given in Eq. (3b). In order to accurately calculate system bandwidth from experimental data, a stochastic simulated annealing model-updating algorithm is employed to numerically fit experimental data to theory (Eq. (8)) (Duda, *et al*. 2001). The model-updating algorithm updates individual circuit elements for both the tag and reader. A typical model-fitting is shown in Fig. 11 for one set of experimental data; it can be observed that the stochastic simulated annealing algorithm can identify tag and sensor equivalent circuit parameters to achieve accurate numerical fitting. Upon determining the resistance, capacitance, and inductance of the sensor tag under different pH buffer solutions, one can then calculate, using Eq. (3b), the change in bandwidth of the system, where the results are plotted in Fig. 12. From Fig. 12, it is apparent that the bandwidth of the wireless pH sensor changes from 270 to 25 Hz as pH increases from 1 to 10.

4.3. Patterning of coil antennas in SWNT-based thin film sensors

Research to fabricate highly conductive thin films using the layer-by-layer self-assembly method is currently underway. It is hypothesized that while carbon nanotubes exhibit near-ballistic transport-type electronic behavior (Baughman, *et al.* 2002), the deposition of other polyelectrolyte species during LbL greatly reduces bulk film conductivity (Loh, *et al.* 2007b). However, through the incorporation of metallic nanoparticles (e.g. gold) within a polymer matrix, Liu, *et al.* (1998) have successfully fabricated LbL films with bulk metal conductivity. Through the addition of carbon nanotubes and a variety of polyelectrolyte species, it is hoped that conductive coil antennas with embedded sensing transduction mechanisms can be achieved in a single LbL assembly process.

Fabrication of carbon nanotube-gold nanoparticle LbL thin films begins by preparing a new set of polycationic and polyanionic solutions. First, by dissolving 1.0 mg/mL of $HAuCl_4$ (Alfa Aesar) in a 1.0 wt.% PVA polycationic solution, gold nanoparticles are formed upon reducing $HAuCl_4$ with 0.1 M

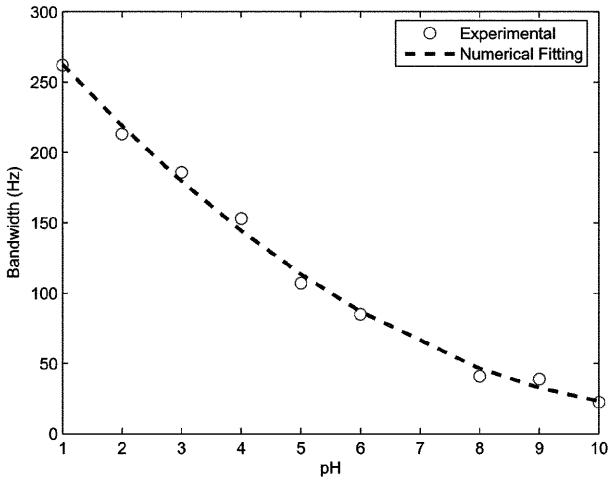

Fig. 12 $(SWNT\text{-}PSS/PANI)_{50}$ thin film parallel resonant circuit shows considerable bandwidth change due to applied pH buffer solution

sodium borohydride ($NaBH_4$) solution (similar to the procedure reported by Zhang, *et al.* 2006). Upon vigorous stirring for 10 min, a pink solution is formed, indicating the completion of preparing the polycationic gold nanoparticle solution (denoted as GNP-PVA). As opposed to using PSS for surfactant steric stabilization of SWNTs, sodium dodecyl sulfate (SDS, $M_w \approx 288.38$, Sigma-Aldrich) is employed for its smaller molecular size and high nanotube deposition density during LbL. Furthermore, preparation of SWNT-SDS dispersed suspensions only require the use of 180 min of ultrasonication bath (no need for using the high-energy probe sonicator), thereby preserving the mechanical and electrical properties of these carbon nanotubes.

Once the polycationic GNP-PVA and polyanionic SWNT-SDS solutions are prepared, the LbL method continues by sequentially dipping a charged glass substrate in these solutions (as described in Section 3). The SEM image of an $(SWNT\text{-}SDS/GNP\text{-}PVA)_2$ thin film is presented as evidence for the

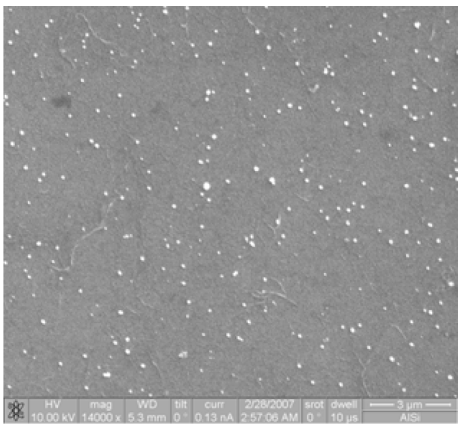

Fig. 13 A scanning electron microscope (SEM) image of an $(SWNT\text{-}SDS/GNP\text{-}PVA)_2$ thin film showing the deposition of both SWNTs and GNPs (bright dots)

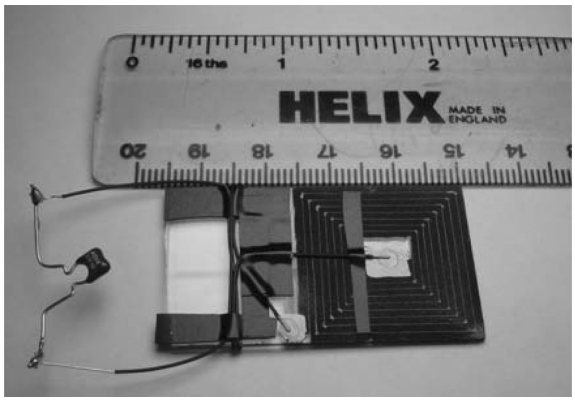

Fig. 14 Picture of patterned $(SWNT\text{-}SDS/GNP\text{-}PVA)_{50}$ thin film coil antenna connected to a 0.1 μF capacitor to form a series resonant circuit

successful deposition of both carbon nanotubes and gold nanoparticles even only after two LbL bilayers (Fig. 13). Upon film fabrication, these $(SWNT\text{-}SDS/GNP\text{-}PVA)_{50}$ thin films are patterned into conductive coil antennas via high-precision mechanical cutting as shown in Fig. 14. In fact, preliminary two-point resistance measurements of these $(SWNT\text{-}SDS/GNP\text{-}PVA)_{50}$ thin film coil antennas suggest 4 to 5 times lower resistance than the aforementioned strain and pH thin film sensors (Loh, *et al*. 2007b). Although film conductivity is greatly enhanced through the incorporation of GNPs and the SDS surfactant for nanotube dispersion and deposition, the coil antenna remains limited by a moderate resistance. After connecting the $(SWNT\text{-}SDS/GNP\text{-}PVA)_{50}$ coil antenna in series with a 0.1 μF capacitor to form a series resonant circuit (Fig. 14), the bandwidth of this system still remains too high for any potential wireless communications (as governed by Eq. (3a)).

Nevertheless, to validate that the patterned coil antenna indeed does behave as an inductor, the series resonant circuit of Fig. 14 is connected to the Solartron 1260 impedance gain/phase analyzer to measure its complex impedance over a range of frequencies. From Eq. (6), one can then deduce the equivalent complex impedance of a series resonant circuit (which is simply the summation of the impedances of the inductor, its series resistance, and the capacitor) as given in Eq. (12).

$$Z = Z_L + Z_R + Z_C \tag{12}$$

where Z_L, Z_R, and Z_C is given in Eq. (6). From Eq. (12) and Fig. 15, it is apparent that resonance will occur when a dip is observed in the impedance magnitude-frequency Bode plot. For the aforementioned series resonant circuit, the resonant frequency is identified as approximately 417 kHz.

In the near future, the fabrication of highly conductive GNP-based LbL thin films will continue. As evident from the SEM image of Fig. 13, the deposition of GNPs is sparse throughout the film surface. It is anticipated that by synthesizing smaller-sized GNPs with diameters between 2 to 25 nm using thiocyanate or sodium citrate, dense GNP deposition (up to 1800 nanoparticles per μm^2) can be achieved to yield films characterized by higher conductivity (Jiang, *et al*. 2004). Alternatively, MEMS processes can be employed to sputter thin copper coils onto LbL substrates to form a wireless antenna upon which thin films can be adsorbed.

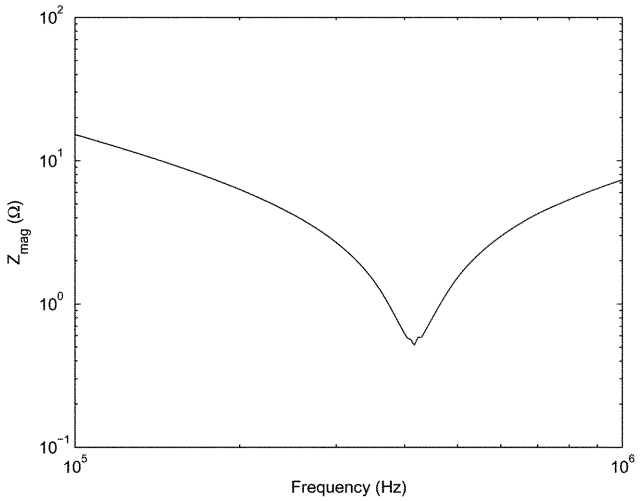

Fig. 15 Experimental RFID reader response collected from $(SWNT\text{-}SDS/GNP\text{-}PVA)_{50}$ thin film coil antenna coupled with a 0.1 μF capacitor

5. Conclusions

In this study, a layer-by-layer self-assembly technique is employed to fabricate carbon nanotube-based thin film passive wireless strain and pH sensors. It has been demonstrated that by selecting different polyelectrolyte species used during thin film assembly, different sensing mechanisms can be encoded within each thin film. First, by depositing SWNTs dispersed in PSS and PVA onto a conformable PET substrate, a capacitive strain sensor is produced. When coupled to a 28 AWG magnetic wire coil antenna and strained to ±10,000 μm/m, the passive wireless sensor can be wirelessly interrogated while exhibiting decreasing resonant frequency with increasingly applied strain. The overall sensitivity of the prototype passive wireless strain sensor is approximately 0.427 Hz/μm-m^{-1}. On the other hand, wireless pH sensing is accomplished with thin films consisting of SWNTs dispersed in PSS and PANI. As different solutions are pipetted into a plastic well mounted above the film surface, the resistive thin film sensor coupled to a parallel resonant circuit exhibits bandwidth change from 270 to 25 Hz as pH scales from 1 to 10. Since the strain and pH sensing mechanism is different (characteristic frequency and bandwidth change, respectively), these sensors can be coupled within one parallel resonant circuit to yield a multifunctional passive wireless sensor.

In an effort to develop a complete thin film wireless sensor, research to produce highly conductive LbL thin films patterned as inductive coils is currently underway. As opposed to just using carbon nanotubes during film fabrication, gold nanoparticles have been successfully integrated with LbL thin films to show a 4 to 5 fold increase in bulk film conductivity. However, inductive coupling between the reader and tag requires further increases in film (LbL coil antenna) conductivity. In the near future, different methods for synthesizing smaller-sized GNPs (2 to 25 nm) will be employed to assist the dense deposition of GNPs during LbL. Nevertheless, the current patterned thin film $(SWNT\text{-}SDS/GNP\text{-}PVA)_{50}$ antenna coupled to a 0.1 μF capacitor does exhibit series resonant circuit behavior, thereby showing great promise for potential wireless communications with LbL assembled thin film sensors.

Acknowledgements

This research is supported by the National Science Foundation (Grant Number CMMI – 0528867 under program manager Dr. Shih-Chi Liu). The authors would like to express their gratitude to Professor Victor Li and the ACE-MRL group for offering access to the MTS-810 load frame during the experimental phase of this study. Furthermore, the authors would also like to thank Dr. Nadine Wong Shi Kam for providing assistance with processing PANI.

References

Baughman, R. H., Zakhidov, A. A., and de Heer, W. A. (2002), "Carbon nanotubes – the route towards applications", *Science*, **297**(5582), 787-792.

Bernhard, J. T., Hietpas, K., George, E., Kuchima, D., and Reis, H. (2003), "An interdisciplinary effort to develop a wireless embedded sensor system to monitor and assess corrosion in tendons of prestressed concrete girders", *Proceedings of IEEE Topical Conference on Wireless Communication Technology*, 241-243.

Celebi, M. (2002), "Seismic instrumentation of buildings (with emphasis on federal buildings)", Technical Report No. 0-7460-68170, United States Geological Survey, Menlo Park, CA.

Decher, G. (1997), "Fuzzy nanoassemblies: toward layered polymeric multicomposites", *Science*, **277**(29), 1232-7.

Doebling, S. W., Farrar, C. R., and Prime, M. B. (1998), "Summary review of vibration-based damage identification methods", *Shock Vib. Digest*, **30**(2), 91-105.

Duda, R. O., Hart, P. E., and Stork, D. G. (2001), *Pattern Classification*, Wiley, New York, NY.

Farrar, C. R. (2001), "Historical overview of structural health monitoring", Lecture Notes on Structural Health Monitoring using Statistical Pattern Recognition, Los Alamos Dynamics, Los Alamos, NM.

Finkenzeller, K. (2003), RFID Handbook Fundamentals and Applications in Contactless Smart Cards and Identification, Wiley, West Sussex, England.

Jiang, C., Markutsya, S., and Tsukruk, V. V. (2004), "Collective and individual plasmon resonances in nanoparticle films obtained by spin-assisted layer-by-layer assembly", *Langmuir*, **20**(3), 882-890.

Kotov, N. A. (2001), "Ordered layered assemblies of nanoparticles", *MRS Bulletin*, **26**(12), 992-7.

Lee, Y. (1998), "RFID coil design", Microchip AN678, 1-18.

Liu, Y., Wang, Y., and Claus, R. O. (1998), "Layer-by-layer ionic self-assembly of Au colloids into multilayer thin-films with bulk metal conductivity", *Chemical Physical Letters*, **298**(4-6), 315-319.

Loh, C-H., Lynch, J. P., Lu, K-C., Wang, Y., Chang, C-M., Lin, P-Y., and Yeh, T-H. (2007a), "Experimental verification of a wireless sensing and control system for structural control using MR dampers", *Earthq. Eng. Struct. Dyn.*, **36**(10), 1303-1328.

Loh, K. J., Kim, J., Lynch, J. P., Wong Shi Kam, N., and Kotov, N. A. (2007b), "Multifunctional layer-by-layer carbon nanotube-polyelectrolyte thin films for strain and corrosion sensing", *Smart Mater. Struct.*, **16**(2), 429-438.

Loh, K. J., Lynch, J. P., Shim, B., and Kotov, N. A. (2008), "Tailoring piezoresistive sensitivity of multilayer carbon nanotube composite strain sensors", *J. Intell. Mater. Sys. Struct.*, **19**(7), 747-764.

Lynch, J. P. and Loh, K. J. (2006), "A summary review of wireless sensors and sensor networks for structural health monitoring", *Shock Vib. Digest*, **38**(2), 91-128.

Lynch, J. P., Sundararajan, A., Law, K. H., Kiremidjian, A. S., Kenny, T. W., and Carryer, E. (2003), "Embedment of structural monitoring algorithms in a wireless sensing unit", *Struct. Eng. Mech.*, **15**(3), 285-297.

Lynch, J. P., Wang, Y., Loh, K. J., Yi, J-H., and Yun, C-B. (2006), "Performance monitoring of the Geumdang Bridge using a dense network of high-resolution wireless sensors", *Smart Mater. Struct.*, **15**(6), 1561-1575.

Mita, A. and Takahira, S. (2002), "Health monitoring of smart structures using damage index sensors", *Proceedings of SPIE – Smart Structures and Materials*, **4696**, 92-99.

Mita, A. and Takahira, S. (2003), "A smart sensor using a mechanical memory for structural health monitoring of a damage-controlled building", *Smart Mater. Struct.*, **12**(2), 204-209.

Mita, A. and Takahira, S. (2004), "Damage index sensors for smart structures", *Struct. Eng. Mech.*, **17**(3-4), 331-346.

Moore, M., Phares, B., Graybeal, B., Rolander, D., and Washer, G. (2001), "Reliability of visual inspection for highway bridges", Technical report no. FHWA-RD-01-020, Federal Highway Administration (FHWA), Washington, DC.

Njord, J. R. and Meyer, M. D. (2006), "Critical issues in transportation", Transportation Research Board of the National Academics, 1-13.

Simonen, J. T., Andringa, A. A., Grizzle, K. M., Wood, S. L., and Neikirk, D. P. (2004), "Wireless sensors for monitoring corrosion in reinforced concrete members", *Proceedings of SPIE – Smart Structures and Materials*, **5391**(1), 587-596.

Sodano, H. A., Inman, D. J., and Park, G. (2004), "A review of power harvesting from vibration using piezoelectric materials", *Shock Vib. Digest*, **36**(3), 197-205.

Spencer, Jr., B. F., Ruiz-Sandoval, M. E., and Kurata, N. (2004), "Smart sensing technology: opportunities and challenges", *Struct. Cont. Health Monit.*, **11**(4), 349-368.

Straser, E. G. and Kiremidjian, A. S (1998), "A modular, wireless damage monitoring system for structures", Technical report no. 128, John A. Blume Earthquake Engineering Center, Stanford University, Stanford, CA.

Tanner, N. A., Wait, J. R., Farrar, C. R., and Sohn, H. (2003), "Structural health monitoring using modular wireless sensors", *J. Intell. Mater. Sys. Struct.*, **14**(1), 43-56.

Todd, M. (2005), "Different approaches towards deploying SHM sensor arrays", *Proceedings of the 5th International Workshop on Structural Health Monitoring*, 1594-1601.

Zhang, M., Su, L., and Mao, L. (2006), "Surfactant functionalization of carbon nanotubes (CNTs) for layer-by-layer assembling of CNT multi-layer films and fabrication of gold nanoparticle/CNT nanohybrid", *Carbon*, **44**(2), 276-283.